The Bjerknes Effect: Explaining Pulsed-Flow Behavior in Bubble Columns

Y. G. Waghmare, F. Carl Knopf, and Richard G. Rice
Dept. of Chemical Engineering, Louisiana State University, Baton Rouge, LA 70803

DOI 10.1002/aic.11200
Published online May 22, 2007 in Wiley InterScience (www.interscience.wiley.com).

New experimental data for a range of gas velocities from 0.1 to 1.5 cm/s are explained by an elementary theory that combines the effect of bubble retardation owing to Bjerknes forces with the breakage relationship of Hinze in a pulsed-bubble column. A frequency range from 10 to 30 Hz, and two amplitudes of fluid oscillation were used in the 8.9 cm column: 1.66 and 2.46 mm. Experimental values of volumetric mass-transfer coefficient for oxygen dissolution followed predictions of theory using a modified penetration model. A new phenomenon was observed and was predictable from theory, namely "flooding", which arises when bubbles are partially or fully retarded by Bjerknes forces at the point of injection. Under flooding conditions, transport enhancement levels off as frequency or amplitude is increased. Bubble-size distribution was measured as a function of frequency, and the calculated Sauter-mean diameter was satisfactorily fitted by the Hinze breakage formula. © 2007 American Institute of Chemical Engineers *AIChE J,* 53: 1678–1686, 2007
Keywords: liquid pulsation, mass transfer, bubble column

Introduction

Recent data[1,2] taken from pulsed bubble-column reactors (BCR) showed several interesting and unexpected properties relative to the enhanced behavior of mass-transfer coefficient and column voidage (holdup). For both mass transfer and voidage, peaking occurred when a flexible piston was used to impart pulsations, but sigmoidal responses arose when a solid piston was used to pulse the liquid phase. The former response characteristics were explained as a result of elastic dynamics arising from the flexible piston. However, the response from the solid piston was only quantified by correlation using power per unit mass, with passing reference to possible effects arising from Bjerknes forces.

We have now uncovered a simplified, one-dimensional (1-D) theory to predict the curious effects using the solid piston. New data have been produced to test the theory, with a range of superficial-gas velocities.

Correspondence concerning this article should be addressed to R. G. Rice at rrice007@centurytel.net or F. C. Knopf at knopf@Isu.edu.

Theory

An expression to compute the time average force on a bubble in a vertically vibrating liquid column was derived by Buchanan et al.[3] some time ago. These authors were more interested in the "entrainment" of bubbles from the top unstable interface of a vibrating column of water, and they provided approximate verification for this entrainment as a function of frequency and amplitude. This was followed by work describing mass transfer into reacting solutions under vibrating conditions.[4] Later, Jameson[5] and Lemcoff and Jameson[6] studied the so-called resonant-bubble contactor in mass-transfer applications. A vibrating slurry reactor was also studied.[7] None of these led to a general theory to explain the enhanced transport observed.

A general expression for the time-averaged force on a submerged bubble (after Bjerknes[8]) is given by

$$\langle F \rangle = \rho \left(V_0 g - \frac{A\omega^2}{2} \Delta V_{\max} \right) \tag{1}$$

where the second term is the induced Bjerknes "kinetic buoyancy" force. A bubble experiences a force in an acceler-

ating liquid in the direction of the acceleration, and is the product of the mass of liquid displaced and the imposed acceleration. In vertical pulsation, the bubble volume is greater at the top of the stroke (smaller hydraulic head) than at the bottom, so the net difference of this kinetic buoyancy acts downward against gravity. When the two buoyancy forces are equal, so that, $\langle F \rangle = 0$ the bubble is held stationary, that is, it oscillates around a fixed position.

The term $\Delta V_{\max}$ represents the maximum volume amplitude of the bubble around the mean of V_o. Buchanan et al.[3] derived the following expression to calculate $\Delta V_{\max}$

$$\frac{\Delta V_{\max}}{V_o} = \frac{\rho h \omega^2 A}{P_o + \rho h g - \rho h \omega^2 A} \tag{2}$$

where h is the height above the bubble, and P_o is the pressure at the top interface. When P_o is atmospheric or larger, so that under most conditions $P_o > (\rho h g - \rho h \omega^2 A)$, hence, we shall take

$$\frac{\Delta V_{\max}}{V_o} \cong \frac{\rho h \omega^2 A}{P_o} \tag{3}$$

Here, liquid amplitude A has been assumed to be independent of vertical position. Earlier, it was shown experimentally that amplitude of liquid pulsation is essentially the same as the cam amplitude.[2] When Eq. 3 is inserted into Eq. 1, we find

$$\langle F \rangle = \rho V_o \, g \left(1 - \frac{1}{2} \frac{(\rho h) A^2 \omega^4}{g \, P_o} \right) = \rho V_o \, g (1 - M(h)) \tag{4}$$

where

$$M(h) = \frac{1}{2} \frac{(\rho h) A^2 \omega^4}{g \, P_o} \tag{5}$$

which takes a value of unity to cause the bubbles to stop rising. The effect on the time-averaged bubble-rise velocity can be inferred from an average-force balance including drag

$$\langle F \rangle = \frac{1}{2} \rho U^2 C_D (\pi R^2) \tag{6}$$

Predicting Voidage

We wish to predict column voidage arising from the effects of pulsation. The retardation of rise velocity is key. In this work, we shall use the drag expression after Kunii and Levenspiel[9]

$$C_D = \frac{10}{\sqrt{\mathrm{Re}}} \tag{7}$$

which is valid for $\mathrm{Re} < 500$.

Inserting this into Eq. 6, and using Eq. 4 for an assumed spherical bubble yields

$$\frac{U}{d} = \left(\frac{2g}{15\sqrt{\upsilon}} \right)^{2/3} [1 - M(h)]^{2/3} \tag{8}$$

where d denotes bubble diameter. This expression shows as $M(h) \to 1$, then $U \to 0$, as required.

For batch systems of the type we have used,[1,2] and for dilute gas holdup, we can write

$$\varepsilon = \frac{U_{og}}{U} \tag{9}$$

which connects gas voidage to gas superficial velocity U_{og} and gas-rise velocity U.

Inserting the rise velocity from Eq. 8 gives an expression to calculate voidage at a position h from the top interface

$$\varepsilon(h) = \frac{U_{og}}{d \left[\frac{2g}{15\sqrt{\upsilon}} (1 - M(h)) \right]^{2/3}} \tag{10}$$

It can be seen in this expression that a singularity arises when $M(h) = 1$. One expects to see a spike in voidage at such points, or bubble clustering.[10,11] As we shall show, our experiments were operated such that $M(h) < 1$. Moreover, an average voidage was measured so the earlier expression must be averaged over the column length. We shall take the bubble size under oscillating conditions to be of the Hinze[12] type, so that

$$d = k \frac{\left(\frac{\sigma}{\rho} \right)^{3/5}}{P_m^{2/5}} \tag{11}$$

The Hinze formula is based on the bubble breakage process in turbulent flows. In the current work, effects of the bubble to bubble coalescence are neglected. The constant k was given in the review of Taitel et al.[13] for gas-liquid systems as 1.14, and was later determined by experiments to take a value of 1.67, using liquid jets to split bubbles by shearing, as reported by Lewis and Davidson[14] (see Table 1). The size reported by these authors represented the maximum stable-bubble size for the breakup of bubbles by turbulent forces. We have made experiments (to be discussed) using high-speed photography to find the Sauter-mean diameter for this experimental program, and the value of the fitted k was found to be 1.70, remarkably close to the value reported by Lewis and Davidson.[14] We shall use the value 1.70 for k in the remainder of the development.

As before,[1,2] we shall take the power per unit mass as*

$$P_m = \left(g U_{og} + \frac{1}{2} A^2 \omega^3 \right) \tag{12}$$

which represents the two contributions from, first, gas injection, and second, liquid oscillation.

The clever combination of theory and experiment in the work of Lewis and Davidson[14] to cause shear induced splitting of bubbles, lends strong support to our contention that bubble breakage in oscillating flow is mainly by shear, and not by eddy effects. Moreover, they showed that the Hinze formula is also applicable to shear breakage, with a different multiplier (1.67) relative to the fitted constant of Hinze (0.725). So, the same power can be used to form eddies (at the tip of impellers, or around baffles), or to cause high-shear rates: either can be the source for breaking bubbles, depending on the configuration of equipment.

*Equation 12 represents the maximum power per unit mass in a cycle, since the transient expression is $P_m(t) = g U_{og} - A^2 \omega^3 \sin(\omega t) \cos(\omega t)$, hence, a maximum for breakage purposes occurs when $\tan(\omega t) = -1$, which finally yields the result in Eq. 12.

Table 1. Summary of Various Values of Premultiplier k in the Hinze Formula Found in Literature

Investigators	Conditions	k	Characteristic Diameter
Hinze[12]	Turbulent flow	0.725	Maximum stable diameter
Taitel et al.[13]	Turbulent flow	1.14	Maximum stable diameter
Lewis and Davidson[14]	Shear flow	1.67	Maximum stable diameter
This work	Oscillating flow	1.7	Sauter mean diameter

Inserting the previous expression for bubble size, and using the earlier power formula, the local voidage in a plane at distance h from the top interface is found from Eq. 10 to be

$$\varepsilon(h) = \frac{U_{og}\left[gU_{og} + \frac{1}{2}A^2\omega^3\right]^{2/5}}{1.7\left(\frac{\sigma}{\rho}\right)^{3/5}\left[\frac{2g}{15\sqrt{v}}(1 - M(h))\right]^{2/3}} \tag{13}$$

To find the average voidage for the column as a whole, we integrate the local value over the total emulsion height H from the gas injector to the top interface

$$\langle\varepsilon\rangle = \frac{1}{H}\int_0^H \varepsilon(h)dh \tag{14}$$

which yields

$$\langle\varepsilon\rangle = \frac{\left(\frac{15}{2}\right)^{2/3}}{1.7}\frac{U_{og}\left[gU_{og} + \frac{1}{2}A^2\omega^3\right]^{2/5}}{\left(\frac{\sigma}{\rho}\right)^{3/5}\left(\frac{g}{\sqrt{v}}\right)^{2/3}}E(M) \tag{15}$$

and

$$E(M) = \frac{3}{M}\left[1 - (1 - M)^{1/3}\right] \tag{15a}$$

where M is the $M(h)$ evaluated at total liquid column height H, and is given as

$$M = \frac{1}{2}\frac{(\rho H)A^2\omega^4}{gP_o} \tag{15b}$$

The limits on $E(M)$ are as follows

$$\lim_{M\to 1} E(M) \to 3;\ \lim_{M\to 0} E(M) \to 1 \tag{16}$$

We shall compare predictions from Eq. 15 in the sections to follow.

Predicting Mass-Transfer Coefficient

From our previous work,[1,2] we expect the measured volumetric mass-transfer coefficient to be enhanced. There are two sources of enhancement arising from the applied pulsation:

1. Enhancement caused by bubble breakage, which increases area (the Hinze effect),

2. enhancement arising from bubble retardation, which increases voidage (the Bjerknes effect).

The Bjerknes force also has a third effect, mentioned earlier, which arises when $M \to 1$. We shall call this the "flooding effect", which is similar in many ways to the flooding observed in counter current gas-liquid packed columns. The flooding effect produces a flood line, as we shall see, which is an upper limit to further increases in mass-transfer coefficient.

We assume that the penetration theory, with modifications, is the appropriate starting point to predict mass transport, hence, for spherical bubbles

$$k_L a = \sqrt{\frac{4}{\pi}\frac{D}{t_c}}\left(\frac{6}{d}\ \varepsilon\right) \tag{17}$$

where, d is the Sauter-mean bubble diameter, and the contact time is taken to be

$$t_c = \frac{d}{U} \tag{17a}$$

The vibrating interface may affect transport at higher frequency, but we have ignored it here. Inserting d/U from Eq. 8, and voidage from Eq. 10 yields an expression for local transport coefficient

$$k_L a = \frac{12}{\sqrt{\pi}}\frac{\sqrt{D}\left(\frac{U_{og}}{d^2}\right)}{\left[\frac{2g}{15\sqrt{v}}(1 - M(h))\right]^{1/3}} \tag{18}$$

where again we shall use the Hinze expression in Eq. 11 to calculate bubble size d. To find the average for $k_L a$, we again integrate over the whole volume as

$$\langle k_L a\rangle = \frac{1}{H}\int_0^H (k_L a)dh \tag{19}$$

which gives

$$\langle k_L a\rangle = \frac{12}{\sqrt{\pi}}\left(\frac{15}{2}\right)^{1/3}\frac{U_{og}\sqrt{D}}{\left(\frac{g}{\sqrt{v}}\right)^{1/3}d^2}G(M) \tag{20}$$

where

$$G(M) = \frac{3}{2}\left[\frac{1 - (1 - M)^{2/3}}{M}\right] \tag{20a}$$

with an upper limit of 3/2 when $M = 1$, and lower limit of 1.0 when $M = 0$.

Combining all the constants when d is inserted from Eq. 11 gives

$$\langle k_L a\rangle = K\frac{U_{og}\sqrt{D}\left[gU_{og} + \frac{1}{2}A^2\omega^3\right]^{4/5}}{\left(\frac{\sigma}{\rho}\right)^{6/5}\left(\frac{g}{\sqrt{v}}\right)^{1/3}}G(M) \tag{21}$$

where $K = \frac{\frac{12}{\sqrt{\pi}}\left(\frac{15}{2}\right)^{1/3}}{1.7^2} = 4.58$.

The frequency corresponding to:

$$M = \frac{1}{2}\frac{(\rho H)A^2\omega^4}{g\,P_o} = 1 \tag{22}$$

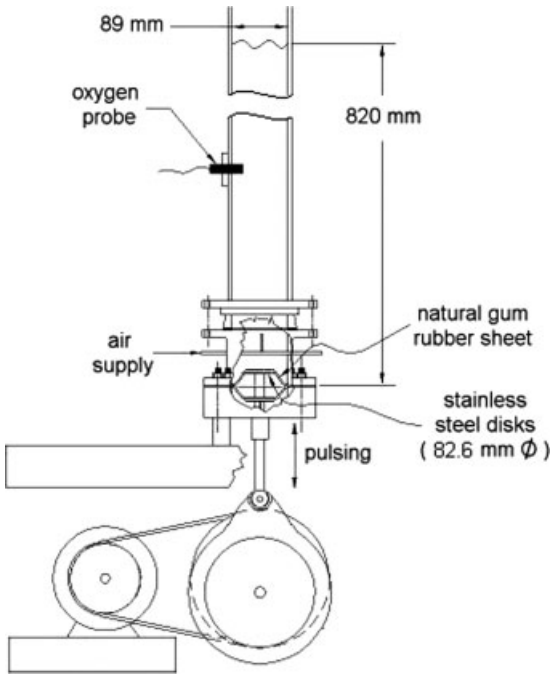

Figure 1. Pulsed bubble-column reactor.

for certain values of A and H will be designated as f_c, which is the critical value at which bubbles stop rising at the point of gas injection (a distance H from the top interface). For this work with $H = 78$ cm, the critical frequency f_c is 27.7 and 22.8 Hz for amplitude of 1.66 and 2.46 mm, respectively.

The theoretical results for voidage and mass-transfer coefficient, represented by Eqs. 15 and 21, respectively, rest on the following explicit and implied assumptions:

1. gas concentration is dilute, $\varepsilon \ll 1$,
2. fluid amplitude is uniform from top to bottom of the column,
3. coalescence rates are small,
4. bubble breakage occurs mainly by shear effects,
5. the expansion and contraction pulsing of bubbles has a small effect on mass transfer (small surface renewal effects).

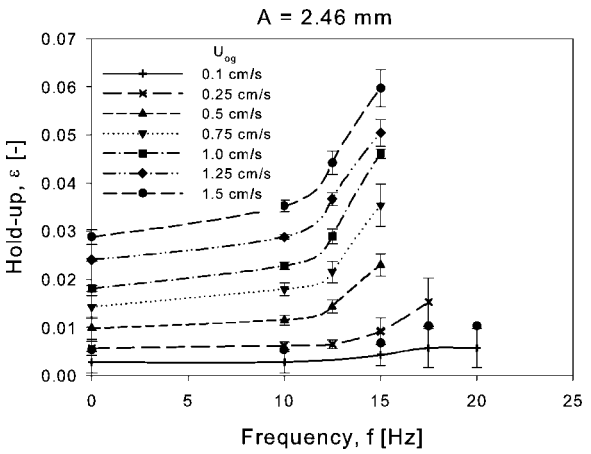

Figure 2. Gas holdup as a function of frequency at various U_{og}; A = 2.46 mm.

Experimental methods

The equipment used is shown in Figure 1. It consists of a Plexiglas® column of 8.9 cm in dia. and 106 cm in height. The base of the column is sealed with a natural gum rubber sheet. The natural gum rubber sheet is clamped between two stainless steel disks. The disks are 8.26 cm in dia., which essentially produces a solid piston at the column base. These disks are directly coupled to an eccentric cam, which is driven by a five horsepower variable speed motor. The motor speed is controlled by an Omron Sysdrive 3G 3JV compact inverter controller. The eccentric cam produces a sinusoidal oscillation to the disks at the base of the column. The system is configured for operation from 0–30 Hz, and amplitudes from 0 to 2.54 mm.

The bubble column reactor was filled with distilled water to a level 78 cm above the injector. Compressed air was injected into the BCR from a single capillary stainless steel injector of 0.75 mm dia. The gas flow rate was controlled by use of a pressure regulator and a needle valve. Low-gas flow rates ($U_{og} < 0.5$ cm/s) were measured by a soap-bubble meter, whereas for high-gas flow rates a totalizing dry test meter (Singer DTM-200) was used. Except for the lowest flow rate, jetting conditions prevailed at the injector tip.

The BCR was operated as batch system with respect to liquid phase (water) and continuous up-flow for the gas phase (air). Experiments were performed for a range of gas superficial velocities, namely, 0.1, 0.25, 0.5, 0.75, 1.0, 1.25, 1.5 cm/s. Frequency was varied from 0 to 30 Hz. Two amplitudes of 1.66 mm and 2.46 mm were investigated.

The gas holdup was determined by the manometric method.[15] Two taps were used, one 11 cm from the piston and the other 77 cm above the piston. The manometer fluid was Meriam Red 295, with a specific gravity of 2.95. A pressure balance on each leg of the manometer allows voidage (ε) to be determined using

$$\varepsilon = \left(\frac{\rho_m - \rho}{\rho}\right)\frac{\Delta x}{X} \tag{23}$$

The height differential in Meriam Red 295, denoted as Δx, was determined using a cathetometer, which provided an accuracy of plus or minus 0.01 mm. Here X is the distance between the two taps.

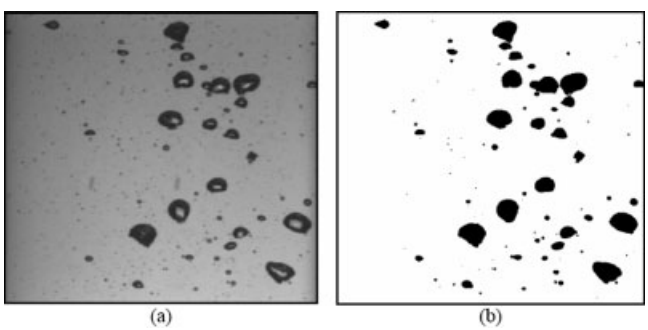

Figure 3. Illustration of image processing during bubble-size distribution measurements.

(a) Raw image, and (b) processed image using ImageJ software.

Table 2. Sauter-Mean Bubble Diameters Taken from BSD at f = 17.5 Hz, A = 1.66 mm, and U_{og} = 0.166 cm/s vs. Column Vertical Position, s

d (cm)	s (cm)
0.69	10.6
0.44	37.7
0.43	53.8
0.41	67.2

It was suspected that large errors may be associated with voidage measurements owing to the fact that applied mechanical oscillations cause a sinusoidal pressure field in the column. Baird[16] showed that under the oscillating conditions, pressure inside the column can be given as

$$P(t) = P_o + \rho(h + A\sin\omega t)(g - A\,\omega^2 \sin\omega t) \qquad (24)$$

Hence, a careful error analysis was made for the voidage experiments. Factors contributing toward error in voidage measurement are: error in manometric reading, error in setting amplitude and frequency, and error in gas flow rate measurements. At an amplitude of 2.46 mm, all the experiments were repeated three times to quantify the error. Figure 2 shows results of voidage measurement experiments at A = 2.46 mm, and at various gas superficial velocities. Average values from these three experiments are shown with error bars of length plus or minus one standard deviation. The error is large at high frequencies near the flood line. In fact it was nearly impossible to measure the voidage at or near the flooding conditions, owing to the high-magnitude of oscillations in the manometric fluid.

Bubble-size distribution (BSD) was measured at different vertical positions in the column. High-speed photographs were made using a high-speed camera (Photron Fastcam PCI-R2). Pictures were taken through a square water box, size 25 cm with height 86 cm, which surrounded the circular column and allowed the bubble swarm to be viewed more clearly. The images from the camera were analyzed using Image J software, which calculates the area of all the bubbles. Figure 3 shows a sample image from the camera and its modified version after the processing. Determined bubble areas were used to calculate bubble-size distribution. Representative bubble size was deduced from the bubble-size distribution curve by calculating the Sauter-mean diameter—the Sauter-mean diameter is the ratio of the third moment to the second moment.

Bubble-size distribution was measured at four different vertical positions along the column. The amplitude of oscillation and the frequency were held constant at 1.66 mm and 17.5 Hz, respectively. Sauter-mean diameter decreases as we move up the column, ultimately reaching an equilibrium value as shown in Table 2. The effect of frequency on bubble-size distribution was studied at vertical position $s = 53.8$ cm. From Figure 4, it can be seen that the size distribution is bimodal until frequency exceeds 15Hz, above which the distributions are normal and unimodal. The peak diameters and the Sauter-mean diameters are not the same, although

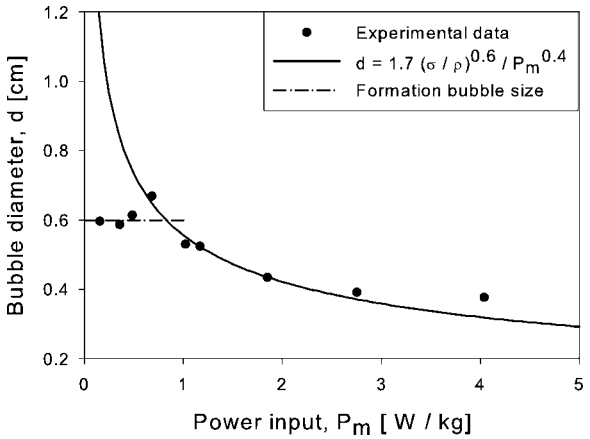

Figure 5. Sauter-mean bubble diameter (measured at vertical position, s = 53.8 cm) vs power input, showing Hinze type of bubble breakage.

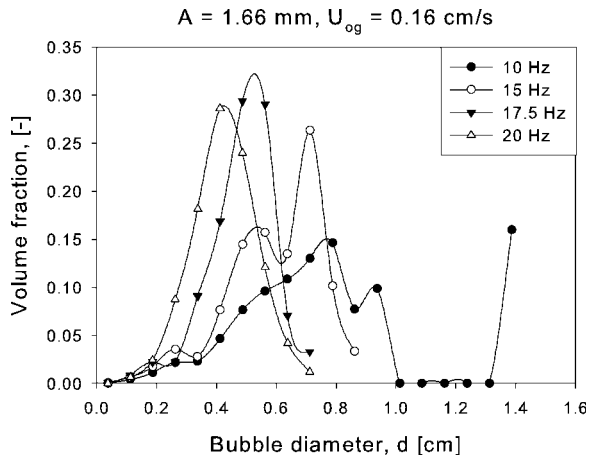

Figure 4. Bubble-size distribution as a function of frequency at a vertical position s = 53.8 cm; A = 1.66 mm, U_{og} = 0.16 cm/s.

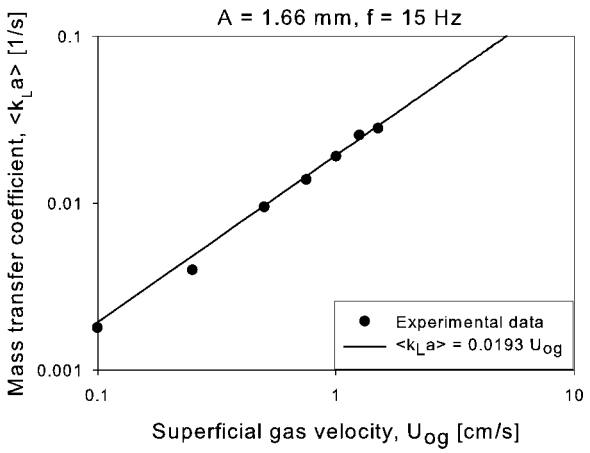

Figure 6. Illustrating the linear dependence on U_{og} according to theory (Eq. 21).

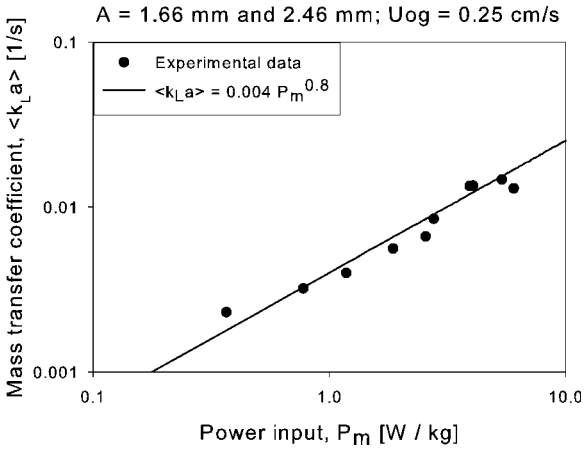

Figure 7. Illustrating $\langle k_L a \rangle$ dependence on $P_m^{0.8}$ according to theory (Eq. 21).

differences between the two values become smaller as the distribution narrows, which is the case for higher frequencies. Figure 5 shows the fit for the Hinze multiplier k in Eq. 11 using the Sauter-mean diameter determined from the image analysis. The flat line through the dia. 0.6 cm, indicates the bubble formation size at the nozzle tip. The fit of the Hinze breakage model was quite satisfactory using the Sauter-mean diameter data. It is seen in Figure 5 that when $P_m < 0.5$ W/kg, the birth size of bubbles prevail, while at higher values of power, breakage from turbulence and shear forces[14] determine bubble size using the Hinze formula with $k = 1.70$.

Mass-transfer experiments were performed by measuring dissolved oxygen concentration as a function of time. A dissolved oxygen probe from Cole Palmer (Model 300 mm) and signal conditioner (Model 01971-00) were used. The oxygen probe was placed 32 cm above the injector. Signals from the oxygen probe were directly recorded in a computer using Labview® instrumentation software. Once oxygen concentration data was obtained, then volumetric mass-transfer coefficient was calculated according to the following expression

$$\frac{C(t)}{C^*} = 1 - \exp(-k_L a t) \tag{25}$$

where $C(t)$ is dissolved oxygen concentration at time t, and C^* is saturation concentration of oxygen in the water. A more detailed account of mass-transfer measurements can be obtained in our previous work.[1]

At low-frequencies, the top free surface of the water shows a definite pattern of surface waves. As frequency is increased, at certain combinations of amplitude and frequency, the top surface becomes unstable, starts disintegrating,[17] and the liquid starts sloshing against the walls. This splashing liquid causes entrainment of the gas from the space above. These unstable conditions can be predicted by applying the inviscid theory of Benjamin and Ursell.[18] A viscosity correction was provided by Nyborg and Rogers[11]. Bretsznajker and Pasiuk[19] observed that this unstable liquid surface contributes significantly to the overall mass transfer. To quantify the contribution from the free surface of water, experiments were performed in which no gas was injected at the bottom of the column. Vibrations were applied (A = 2.46mm, f = 17.5 Hz), and oxygen up take was measured. In this case the only possible way of oxygen transfer to the liquid is through the unstable top surface of the water. Even after operating for a long period of time (more than 1 h), no significant dissolved oxygen concentration was observed. Hence, it was concluded that there is little mass-transfer contribution from the top unstable interface. The mass transfer occurs mainly through gas bubbles dispersed in the liquid phase via the gas injector. We have made estimates for mass transfer through the wavy top interface under the worst case to be no more than seven percent of the total transfer during an experiment, provided $f < fc$.

Comparison of Theory and Experiment

Theoretical predictions of voidage and mass-transfer coefficient given by Eq. 15 and 21, respectively, were compared with experimental results. The kinematic viscosity was taken as 0.01 cm^2/s, and oxygen diffusivity in water was taken to be 2.5×10^{-5} cm^2/s.

In Figures 6 and 7, we confirm the predicted linear dependence of $\langle k_L a \rangle$ on U_{og}, and the power/mass dependence as $P_m^{0.8}$, respectively. Earlier work by Harbaum and Houghton[20] showed linear dependence on P_m, which is very similar to the exponent of 0.8 used in this work (see Table 3). Baird and Garstang,[21] Ni and Gao[22] gave dependence on P_m to the power of 0.42, for rather different methods of imposing pulsations in the presence of baffles. They also showed that $\langle k_L a \rangle$ depends on U_{og} to the power of 0.5 and 0.37, respectively. Krishna and Ellenberger[23] observed linear dependence of $\langle k_L a \rangle$ on U_{og}, which matches with this work. In our earlier work,[2] we reported that $\langle k_L a \rangle \propto P_m^{0.4}$ based on $\langle k_L a \rangle$ measurements at a single superficial-gas velocity of 0.5 cm/s. The earlier experiments did not include effects arising from the slowing down of bubbles owing to Bjerknes kinetic buoyancy. This, and the single velocity used, distorted the curve fit, which was based on quite scattered data.

Table 3. Summary of Operating Conditions and Mass-Transfer Coefficient Correlations Available in Literature for Oscillating Bubble Column Reactors. Here, $k_L a \propto P_m^a U_{og}^b G(M)^c$

Investigators	System	f (Hz)	A (mm)	U_{og} (cm/s)	P_m (W/kg)	$k_L a$ (1/s)	a	b	c
Harbaum and Houghton[20]	CO_2–water	20–2000	0.01–1	1.4	0–0.7	0.02–0.06	1	–	0
Baird and Gerstang[21]	Air–water (baffled)	1–1.35	0–94	0.8–2.5	0.1–1.8	0.03–0.17	0.42	0.50	0
Ni and Gao[22]	Air–water (baffled)	1–10	1–12	0.4–1.7	0.03–1.5	0.01–0.08	0.42	0.37	0
Knopf et al.[2]	Air–water	0–30	0–2.46	0.5	0–10	0.004–0.03	0.4	–	0
Krishna and Ellenberger[23]	Air–water	0–120	0–25	0.1–1.5	0–40	0.01–0.05	–	1	0
This work	Air-Water	0–30	0–2.46	0.1–1.5	0–6.0	0.001–0.036	0.8	1	1

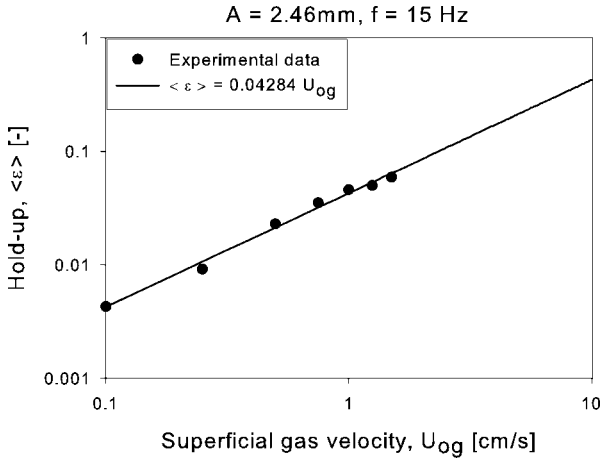

Figure 8. Illustrating the linear dependence on U_{og} according to theory (Eq. 15).

The current theory for $\langle k_L a \rangle$ predicted a squared inverse dependence on bubble size, as shown in Eq. 20. For the Hinze bubble size given by Eq. 11, this means $\langle k_L a \rangle$ is forecast to depend on $P_m^{0.8}$, which appears to be confirmed by our new experiments for varying U_{og}, A and $\omega = 2\,\pi f$. Similarly, Figures 8 and 9 shows linear dependence of ε on U_{og}, and also the voidage dependence on $P_m^{0.4}$.

In Figure 10, we illustrate $\langle k_L a \rangle$ predictions from our theory, using our theoretical constant of 4.58, in comparison with experiments at various U_{og} for amplitudes of 2.46 mm and 1.66 mm, respectively. Figure 10 also illustrates the "flooding line" which is the horizontal line formed at the intersection of f_c (when $M = 1$) with the theoretical curve. The line represents the upper asymptote for $\langle k_L a \rangle$ when bubbles are stopped by Bjerknes forces at the nozzle tip.

The derived constant (K) for $\langle k_L a \rangle$ was stated before as 4.58, while the curve fit yielded 4.45. A total of 81 experimental points were used to fit K. However, the best fitted value of K, which is remarkably close to the theoretical value, only approximates pinpointing the flood condition.

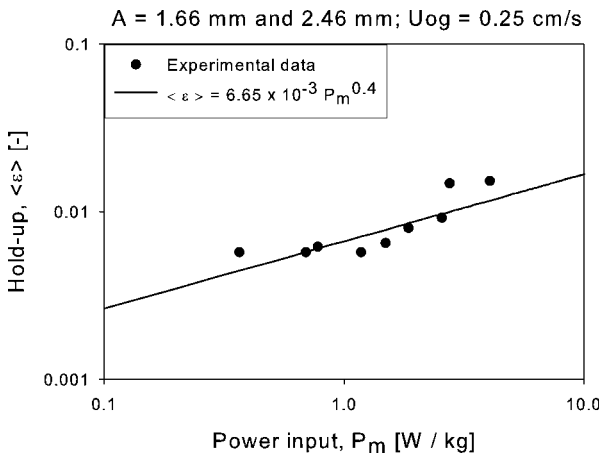

Figure 9. Illustrating voidage dependence on $P_m^{0.4}$ according to theory (Eq. 15).

We have also made a comparison by modifying the Hinze expression, so that $d \to d_c$ as input power gets very large. We have taken the critical bubble size, in the lower limit, to follow Brodkey's[24] law

$$d_c = \left[\frac{0.4\sigma}{(\rho - \rho_g)g}\right]^{1/2} \tag{26}$$

which is the size small enough to maintain sphericity, and, thus, prevent agglomeration owing to turbulent eddies. It would seem adding such a constant to the Hinze expression would be a reasonable proposition, to prevent the rather physically unrealizable state of zero bubble size as $P_m \to \infty$. The addition of d_c to the expression for d in Eq. 11 gave slightly better curve fits, but was not deemed worth the additional complication of one additional parameter. It may be called upon in future.

Figure 11 compares the theoretical curve given by Eq. 15 and the experimental data for voidage measurements. The predicted multiplier for voidage in Eq. 15 was 2.25, while

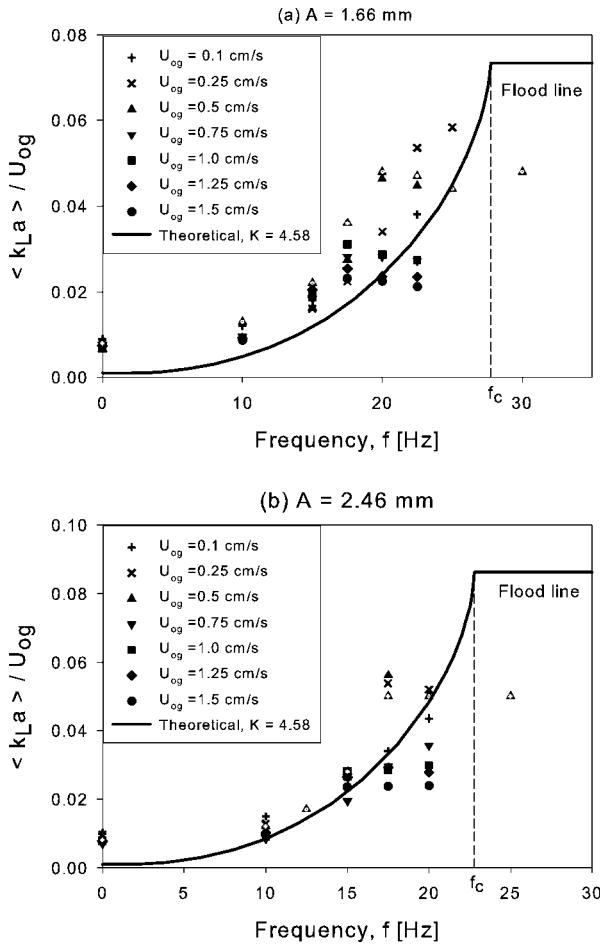

Figure 10. Comparison between theoretical predictions and experimental data for mass transfer coefficients at various U_{og}.

Solid line shows theoretically predicted curve according to Eq. 21 with $K = 4.58$. Open triangle show data taken from Ma[25]; (a) $A = 1.66$ mm, (b) $A = 2.46$ mm.

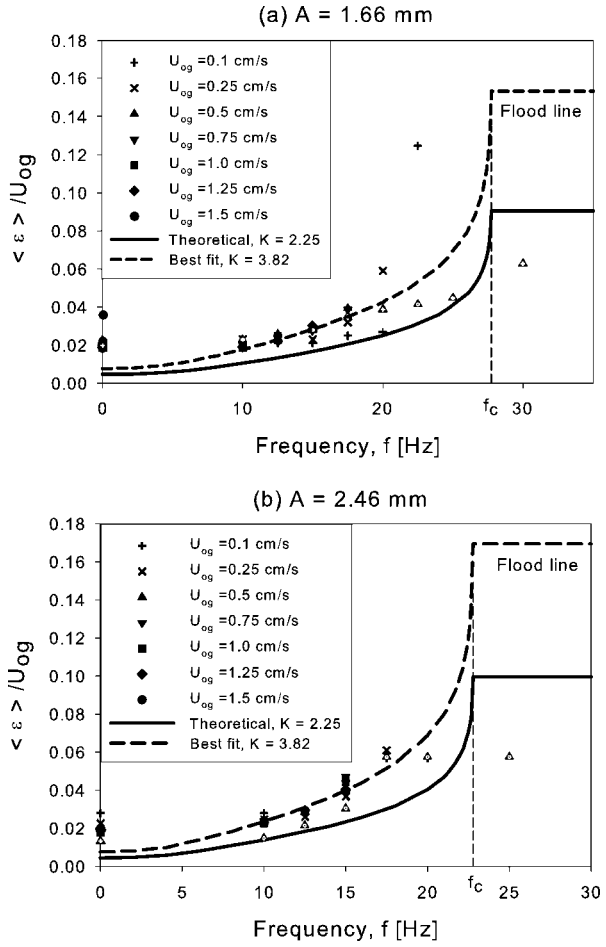

Figure 11. Comparison between theoretical predictions and experimental data for gas hold-up at various U_{og}.

Solid line shows theoretically predicted curve according to Eq. 15 with $K = 2.25$. Dashed line indicates a best fit with premultiplier $K = 3.82$. Open triangle show data taken from Ma[25]. (a) $A = 1.66$ mm, (b) $A = 2.46$ mm.

the data best fit gave 3.82. Hence, we use the value of 2.25 for the theoretical curve in Figure 11, where the dashed curve is for the best fit. It is quite remarkable that this theory, which includes several bold assumptions, can track the data so well.

Comments and Conclusions

A rather simple 1-D theory, based on the Bjerknes kinetic buoyancy force, and the Hinze bubble-breakage formula, led to good comparisons with a large number of experiments for voidage and mass-transfer coefficient. An upper limit is pinpointed when bubbles are stopped from rising upward at the injection point, hence, flooding occurs. The theory is strictly applicable to dilute gas systems of low-viscosity liquids (such as water). It is also shown that applied pulsations produce more uniform bubble-size distributions. An extension to viscous systems is currently being studied, along with the effects of a periodic velocity profile depending on local radial position.

Notation

a = interfacial area per unit volume, cm^2/cm^3
A = amplitude of imposed liquid pulsation, cm
C = dissolved oxygen concentration, $gmol/cm^3$
C^* = equilibrium value of dissolved oxygen, $gmol/cm^3$
C_D = drag coefficient, dimensionless
d = bubble diameter, cm
d_C = critical bubble diameter, cm
D = molecular-diffusion coefficient, cm^2/s
$E(M)$ = $\frac{3}{M}[1-(1-M)^{1/3}]$, dimensionless
$\langle F\rangle$ = time-average force, dyne
f = frequency, Hz
f_c = critical frequency when $M = 1$, Hz
g = acceleration from gravity, cm/s^2
$G(\mathrm{M})$ = $\frac{3}{2}\left[\frac{1-(1-M)^{2/3}}{M}\right]$, dimensionless
h = distance from top interface to bubble, cm
H = distance from top interface to gas injector, cm
k = premultiplier from Eq. 11, dimensionless
$k_L a$ = volumetric mass-transfer coefficient, 1/s
$\langle k_L a\rangle$ = average volumetric mass-transfer coefficient under pulsing, 1/s
$M(h)$ = local Bjerknes number, $\frac{1}{2}\frac{(\rho h)A^2\omega^4}{g\,P_o}$, dimensionless
M = Bjerknes number at position H, $\frac{1}{2}\frac{(\rho H)A^2\omega^4}{g\,P_o}$, dimensionless
P = pressure, $dyne/cm^2$
P_o = pressure at top interface, $dyne/cm^2$
P_m = power input per unit mass, W/kg or cm^2/s^3
R = bubble radius, cm
Re = bubble-Reynolds number, $\frac{dU}{\upsilon}$, dimensionless
s = vertical position in the column, cm
t = time, s
t_c = contact time for mass transfer, d/U, s
U_{og} = superficial-gas velocity, cm/s
U = time-average bubble-rise velocity, cm/s
V_o = mean-bubble volume, cm^3
X = distance between the two taps for manometer, cm
Δx = height difference between two arms of the manometer, cm

Greek letters

$\varepsilon(h)$ = local voidage in a plane at h
$\langle\varepsilon\rangle$ = average voidage over column
υ = kinematic liquid viscosity, cm^2/s
ρ = liquid density, g/cm^3
ρ_g = gas density, g/cm^3
ρ_m = manometer fluid density, g/cm^3
σ = surface tension, dyne/cm
ω = frequency, radians/s

Literature Cited

1. Knopf FC, Ma J, Rice RG, Nikitopoulos D. Pulsing to improve bubble column performance: I Low gas rates. *AIChE J*. 2006;52:1103–1115.
2. Knopf FC, Waghmare Y, Ma J, Rice RG. Pulsing to improve bubble column performance: II Jetting gas rates. *AIChE J*. 2006;52:1116–1126.
3. Buchanan RH, Jameson G, Oedjoe D. Cyclic Migration of bubbles in vertically vibrating liquid columns. *IEC fundam.* 1962;1:82–86.
4. Buchanan RH, Teplitsky DR, Oedjoe D. Oxygen absorption in low-frequency vertically vibrating liquid columns. *IEC Proc Des Dev*. 1963;2:173–177.
5. Jameson GJ. Some operating characteristics of the resonant bubble contactor. *Trans I Chem E*. 1966;44:T91–96.
6. Lemcoff NO, Jameson GJ. Solid-Liquid mass transfer in a resonant bubble contactor. *Chem Eng Sci*. 1975;30:313–367.
7. Lemcoff NO, Jameson GJ. Hydrogenation of Acetone in a vibrating slurry reactor. *AIChE J*. 1975;21:730–735.

8. Bjerknes V. Die Kraftfelder. 1st ed. Friedrich Vieweg and Sohn, Braunschweig; 1909.
9. Kunii D, Levenspiel O. *Fluidization engineering*. 1st ed. New York, NY: John Wiley & Sons Inc; 1969.
10. Ellenberger J, van Baten JN, Krishna R. Exploiting the Bjerknes force in bubble column reactors. *Chem Eng Sci*. 2005;60:5962–5970.
11. Nyborg WL, Rodgers A. The motion of liquid inside a closed vibrating vessel. *Biotech Bioeng*. 1967;9:235–256.
12. Hinze JO. Fundamentals of the hydrodynamic mechanism of splitting in dispersion processes. *AIChE J*. 1955;1:289–295.
13. Taitel Y, Bornea D, Dukler AE. Modeling flow pattern transitions for steady upward gas-liquid flow in vertical tubes. *AIChE J*. 1988; 26:345–354.
14. Lewis DA, Davidson JF. Bubble splitting in shear flow. *Trans I Chem E*. 1982;60:283–291.
15. Burns LF. *The effect of reduced surface tension on mass transfer and fluid dynamics in bubble column reactors (BCR)*. Baton Rouge, LA: Louisiana State University. 1995. M.S. Thesis.
16. Baird MHI. Suction due to fluid pulsation. *Can J Chem Eng*. 1970;48:126.
17. Hashimoto H, Sudo S. Surface disintegration and bubble formation in vertically vibrated liquid column. *AIAA J*. 1980;18:442–449.
18. Benjamin TB, Ursell F. The stability of the plane free surface of a liquid in vertical periodic motion. *Proc R Soc Lond A Math Phys Sci*. 1954;225:505–115.
19. Bretsznajder S, Pasiuk W. Absorption in a pulsed column. *Int Chem Eng*. 1964;4:61–66.
20. Harbaum KL, Houghton G. Effects of sonic vibrations on the rate of absorption of carbon dioxide in gas bubbles-beds. *J Appl Chem*. 1962;12:234–240.
21. Baird MHI, Garstang JH. Gas absorption in a pulsed column. *Chem Eng Sci*. 1972;27:823–833.
22. Ni X, Gao S. Scale-up correlation for mass transfer coefficients in pulsed baffled reactors. *Chem Eng J*. 1996;63:157–166.
23. Krishna R, Ellenberger J. Improving gas-liquid contacting in bubble columns by vibration excitement. *Int J Multiphase flow*. 2002;28: 1223–1234
24. Brodkey RS. *The Phenomenon of fluid motion*. 1st ed. Reading, MA: Addison-Wesley Press; 1967.
25. Ma J. *Forced bubble columns*., Baton Rouge, LA: Louisiana State University; 2003. MS Thesis.

Manuscript received July 27, 2006, and revision received Mar. 19, 2007.